ACS APPLIED MATERIALS & INTERFACES

Research Article

www.acsami.org

Electrical Transport and Breakdown in Graphene Multilayers Loaded with Electron Beam Induced Deposited Platinum

Neha Kulshrestha,*[,†] Abhishek Misra,[‡] Nikhil Koratkar,[§] and D. S. Misra[†]

[†]Department of Physics and [‡]Department of Electrical Engineering, Indian Institute of Technology Bombay, Mumbai 400076, India

[§]Department of Mechanical, Aerospace and Nuclear Engineering and the Department of Materials Science and Engineering, Rensselaer Polytechnic Institute, 110 8th Street, Troy, New York, United States

ABSTRACT: We demonstrate here the effect of electron beam induced deposited platinum on the electrical transport through multilayer graphene sheets. Platinum metal is deposited at different positions on the graphene multilayers, i.e., including as well as excluding the bottom contact sites and the change in electrical conductance of the same multilayer graphene sheets before and after platinum deposition is segregated. An improvement in electrical conductance is observed even if the metal is deposited at the part of the graphene sheets that does not touch the bottom gold electrodes, and hence this experimental approach directly demonstrates that the contact improvement is not the sole reason for the improved electrical conduction. The improvement in electrical performance of the graphene sheets is explained in terms of the doping of graphene sheets caused by the charge transfer between the deposited metal and the graphene and thereby modified density of states for electrical conduction. Metal deposition also leads to the increased interlayer interaction of the graphene sheets as revealed by the transmission electron microscopy analysis. Further, two types of breakdown behaviors viz. sharp and stepped breakdowns observed for these graphene devices are explained in terms of the effective graphene−metal contact area. These studies reveal the implications of top metal contact fabrication on graphene for electronic devices.

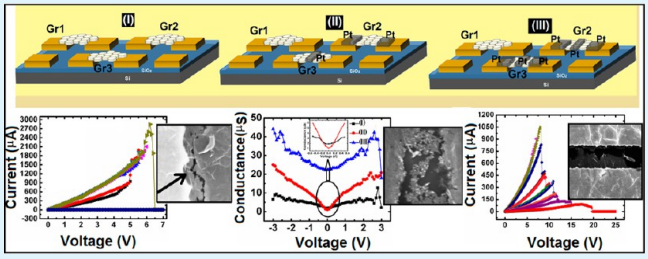

KEYWORDS: *multilayer graphene sheets, electron beam induced deposition, current−voltage characteristics*

1. INTRODUCTION

A graphene−metal interface is ubiquitous in almost all graphene (Gr) devices. In the experimental studies, generally the electrical contact is fabricated by metal deposition on top of the graphene sheets lying on a dielectric.[1,2] Another approach for contact formation is to disperse graphene on already fabricated metal electrodes.[3] It should be noted that the electronic behavior of graphene on metal contacts may be different from that of the metal on graphene case.[4] Nevertheless, in both cases, the sheet of graphene is doped with the charge carriers whether the graphene lie on the metal surface[3,5,6]or is underneath the metal surface[7,8] and this doping affects the graphene's electronic properties.[9] The currently available studies on graphene devices measure its electrical properties after the whole device fabrication including the metal deposition step[1,2,4,7,10−15] and hence the impact of metal−graphene interaction on its electrical behavior before and after metal deposition cannot be isolated. It is important to understand that the electrical measurements performed on such devices not only involve the intrinsic electrical conduction of the graphene sheets but also include the modification (enhancement) caused by the metal induced effects like change in the density of available states by charge transfer and the increased interlayer interaction caused by the intercalation of metal atoms. None of the available studies reported the contribution of the effect of such increased interlayer interaction by metal deposition and just report the electrical conduction of the finally fabricated graphene devices.

In this study, we demonstrate that the effect of the deposited metals is not limited to only the upper one or two layers but can cause increased interaction amongst several layers. This increased interlayer interaction facilitates the vertical tunneling of the charge carriers which leads to the enhanced electrical conduction even at low fields. Further, we quantitatively segregate the change in electrical conductance of the same multilayer graphene sheets before and after Pt deposition. A significant improvement in current is observed after top metal (Pt) deposition on graphene multilayers. This improvement is important in the wake that only the bottom-most graphene sheet in the multilayer flake remains in direct contact with the bottom metal (Au) electrodes and the graphene sheets within the flakes are weakly interacting among themselves. Surprisingly an improvement in electrical conductance is observed even if the metal is deposited on the part of the graphene sheets which do not touch the bottom gold electrodes. Such an improvement is explained in terms of significantly increased interaction among the individual layers caused by the doping from the deposited metal. This finding would have remained ambiguous

Received: February 5, 2013
Accepted: March 13, 2013
Published: March 14, 2013

if the metal was deposited exclusively at the part of the sheets touching the bottom contacts and can be misleadingly attributed to contact improvement.

The experimental approaches presented in this study directly demonstrate the effect of top metal deposition and separate out the contribution due to contact improvement and due to increased interlayer interaction in the overall electrical conduction of the graphene sheets. Further, two types of breakdown behaviors viz. sharp and stepped breakdowns are observed for these graphene sheets. These breakdown behaviors are explained in terms of the effective graphene-metal contact area.

2. RESULTS AND DISCUSSION

The graphene sheets used in the study were produced by thermal exfoliation and reduction of graphite oxide (details can be seen in Experimental Section and in ref 16). The transmission electron microscopic (TEM) images of typical sheets used for the study are shown in Figure 1a, b. The typical

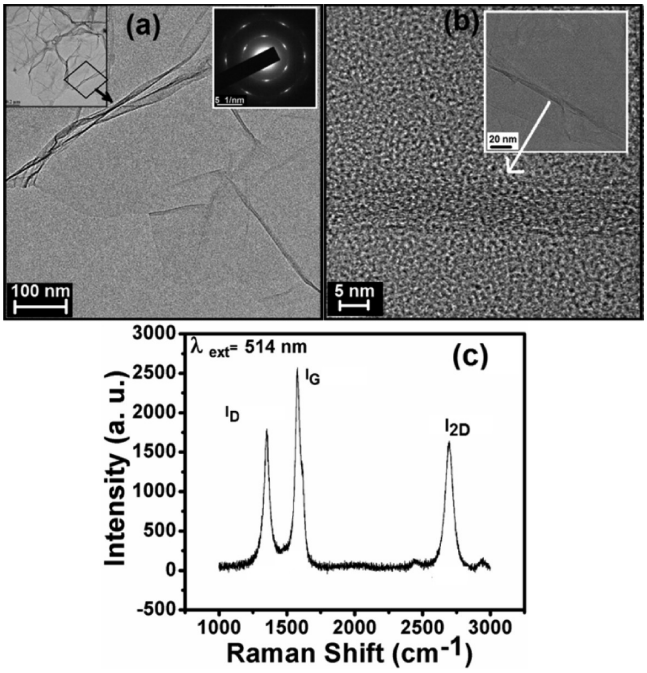

Figure 1. Transmission electron microscopic (TEM) images of typical graphene sheets used for the study: (a) magnified view of folded graphitic layers shown in the left inset while inset at right shows the diffraction pattern; (b) high-resolution TEM image showing the discontinuous and defective nature of the sheets. (c) Raman spectra of the graphene sheets dispersed on gold substrate.

thickness of the graphene sheets used in this study is about ~5-7 nm as verified by HRTEM (Figure 1 and Figure 6 of the manuscript), and cross sectional TEM (X-TEM, not shown here) observations. The thickness of the graphene sheets were consistent for all the graphene flakes used in the study as confirmed by X-TEM imaging of different graphene flakes. The diffraction pattern at the inset of Figure 1a is typical to the folding in graphene layers or the so called graphene scrolls.[17] The Raman spectra of the flakes at $Si/SiO_2/Au$ substrate, obtained at excitation wavelength of 514 nm is shown in Figure 1c. The Raman spectra support the high resolution TEM (HRTEM) information (Figure 1b) about the multilayer, and defective nature of the graphene sheets. The three main peaks, the so called D band, G band and 2D band, typical to the Raman spectra of the graphene sheets are present at 1350, 1579, and 2695 cm^{-1}, respectively. The presence of intense D band is the signature of defects such as edges and foldings present in the graphene samples. The 2D/G peak intensity ratio for these sheets is 0.63, indicating the multilayer nature of the sample.[18]

The experimental procedure used to obtain electrical characteristics of the graphene sheet devices is depicted in Figure 2. In this figure, we depict just three graphene flakes (Gr1, Gr2, and Gr3) on the same substrate. However, several such graphene sheet devices were measured in the similar configurations. The first schematic (I) presents the graphene sheets suspended on the two bottom Au electrodes without any top metal. The second schematic (II) shows the Pt metal deposition on the graphene flakes. At this step (II), the two edges of some flakes (like Gr2) at the bottom (Au) contacts were covered by metal (Pt) deposition, whereas on some other flakes (like Gr3), metal has been deposited at the middle of the spacing between the two gold electrodes. For each of these sheets $I-V$ measurements were performed. At the third step (III), the Pt metal was deposited at the middle between the two electrodes where previously (at step II) only the edges of graphene flakes were covered by Pt, whereas for the flakes on which the Pt at the middle was deposited earlier, now the edges were covered by Pt metal followed by $I-V$ measurements.

The scanning electron microscope (SEM) image of graphene sheets, suspended on two gold electrodes, of around 2 μm separation between them, is shown in Figure 3a. The current–voltage ($I-V$) characteristics of the sheets are shown in Figure 3c, d. The resistance of the graphene sheets, extracted from the $I-V$ curve at low biases is 14.2 kΩ. For voltage higher than 2.0 V, the current has been obtained only for positive biases so as to study the exact breakdown behavior of the sheets (Figure 3d). The current reaches to 2.8 mA at 6.2 V and then abruptly degraded to 2.3 μA at 6.5 V. This current reduction from milli- to microampere range indicates the failure of the current carrying sheets. For the next sweep of 7 V, the vanishing current suggests the breakdown of the device. The breakdown of the device is also confirmed by SEM imaging (Figure 3b). The observed breakdown site of the sheets is towards the left contact electrode. For all the suspended sheet devices in our study, the failure site is always observed near one contact side where the contact area of graphene flakes with bottom contact is less. This breakdown behavior finds its origin in efficient removal of joule heat from the devices and can be understood in terms of the temperature profile for particular device. In general, when a large area of graphene sheet is in contact with bottom metal electrode, the two contacts behave as good heat sinks and breakdown threshold is delayed. However, the two contact areas should be almost symmetric (or of equal heat removal efficiency) in order to expect the breakdown of the sheets in the middle because only then the temperature profile is parabolic with the maximum temperature rise in the middle of the two electrodes.[19,20] In the case depicted in Figure 3, the contact area of graphene sheet is large towards the right electrode, hence the left contact has the higher resistance and greater temperature rise occurs near the left electrode, resulting in breakdown site near this electrode. For the graphene sheet devices having equal contact area on both the contacts, breakdown is observed in the middle.

We now present the effect of Pt metal deposition on the electrical characteristics of the graphene sheets. The local metal

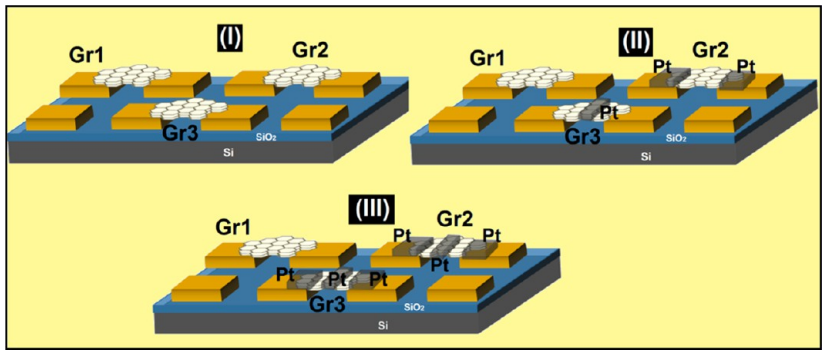

Figure 2. Schematic of the experimental procedure, three Gr sheets (Gr1, Gr2, Gr3) on gold electrodes, dimensions are not to the scale. (I) without any top metal deposition, (II) top metal (Pt) deposition on selected locations on graphene (Gr2 edges and Gr3 middle), and (III) top Pt deposition at Gr2; middle and at the edges of Gr3.

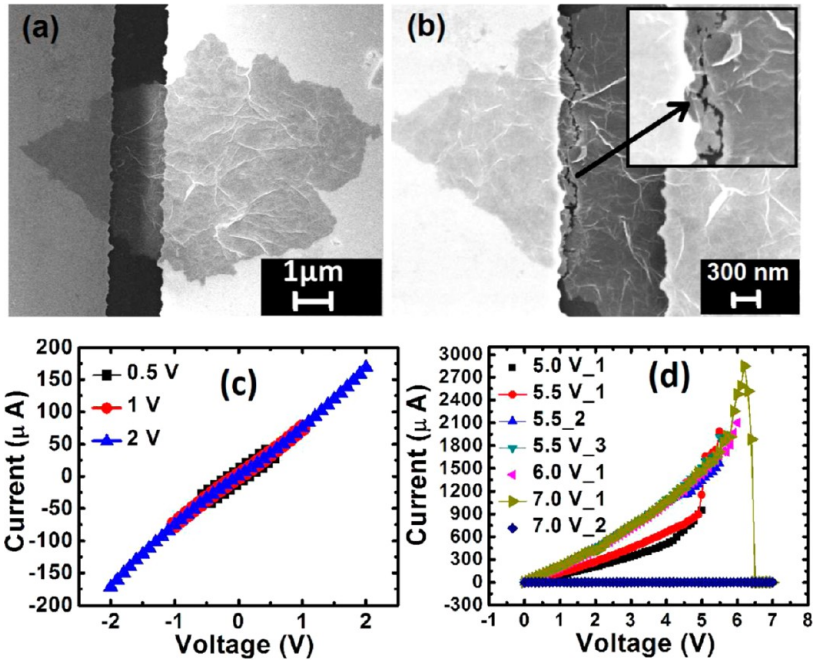

Figure 3. SEM image of graphene sheets suspended between two gold electrodes. (a) before breakdown, (b) after breakdown, (c) *I*–*V* curves of the sheets up to 2 V, (d) *I*–*V* curve of the sheets at higher voltages till breakdown. Repeated voltage sweeps (e. g. 5.5 V_1 and 5.5 V_2) were performed when instability in current (due to burning of different sheets) is observed.

deposition on the sheets has been achieved using electron beam induced deposition (EBID) of Pt (see Experimental Section). The typical thickness of the deposited Pt metal is about 7-10 nm and can be varied by controlling the EBID parameters. This technique allows us to precisely deposit Pt top contacts on the graphene sheets to study the difference in electrical characteristics before and after Pt deposition. For the graphene device shown in Figure 4a, the current at 3 V is found to be 20 μA before any top Pt deposition. After Pt deposition on the sheets at two contacts (visible as dark contrast rectangles at the two sides, Figure 4b) the current increases to 40 μA. The current of the sheets before and after Pt deposition is shown in Figure 4e. At prima facie, this improvement in the current value (doubled compared to the previous one) can be easily explained in terms of the contact improvement as the Pt metal is deposited at the graphene sheets on the two contacts. However, this enhanced conduction may also be due to the increased interlayer interaction as the effect of the deposited metal may not be limited to the top most sheet, especially with the electron beam assisted deposition of metals. To segregate this effect from the contact improvement, we next deposited the Pt is deposited on the part of the same graphene sheet not touching the bottom electrodes (Figure 4c). It is important to mention here that the thickness and dimension of the deposited metal has been kept such as to confine the deposit metal in middle of the electrodes only and to avoid any metal deposition at the junction area. The area of the EBID deposited metal (of thickness 7–10 nm) can be larger than actually defined shape; nevertheless, the extended window due to stray Pt particles does not exceed beyond 100 nm of the actually defined shape.

Interestingly, the deposition of Pt metal even at this location results in a huge improvement in current from a value of 40 μA to 100μA as shown in Figure 4e. It is evident that this improvement cannot be attributed to contact improvement and needs further investigation as will be discussed later in this paper. The conductance–voltage (*G*–*V*) curves for this device (Figure 4a–c) before and after every step of Pt deposition, indicated by I, II, and III, are shown in Figure 4f. After metal

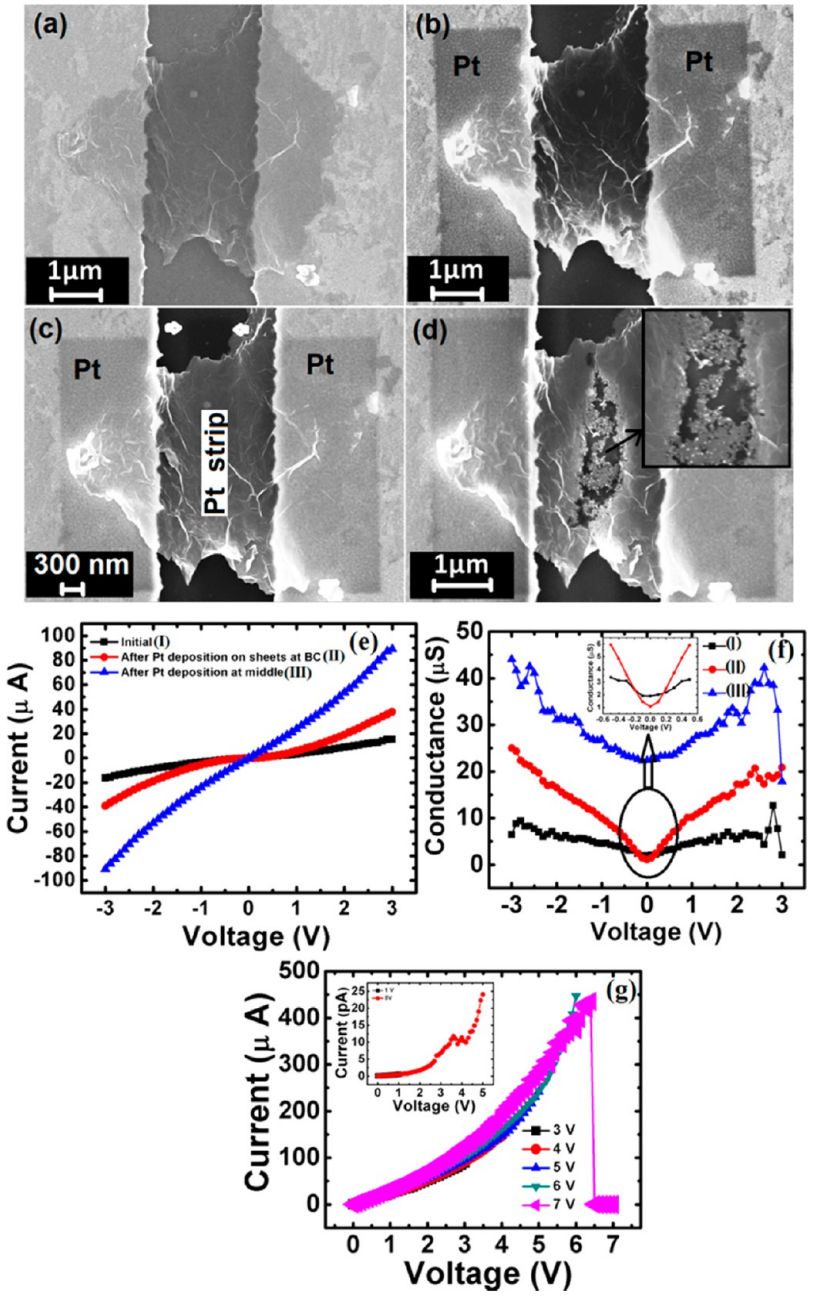

Figure 4. (a) Graphene sheets suspended on two gold electrodes, (b) after Pt metal deposited at the two sides of sheets on bottom electrodes, (c) Pt metal deposition at the middle of the spacing between the two electrodes (visible as the dark contrast in middle), (d) SEM image after the breakdown of the graphene sheet device, Pt nanoparticles formed at the middle of the electrodes are visible (inset shows the magnified view of the Pt nanoparticles). (e, f) $I-V$ and $G-V$ curves of the graphene sheet device corresponding to the situations of Pt metal deposition depicted in a–c, respectively. Inset of f shows the observed negative zero bias conductance marked by encircled region. (g) $I-V$ curves of the graphene sheet device till breakdown, inset shows the negligible but not vanishing current even after the breakdown.

deposition a clear improvement in the average conductance of the sheets has been observed. The improvement in the conductance after Pt deposition at contacts can be attributed to the combined effect of contact improvement and increased interlayer interaction coming because of the doping of the graphene sheets with the Pt metal. The improved conduction after Pt deposition in the middle can only be attributed to the increased interlayer interaction caused by intercalation of Pt metal atoms that dope the graphene sheets. One important observation for this device is the appearance of negative conductance region around zero bias after first Pt deposition as shown in the inset of Figure 4f. Before Pt deposition, the zero bias conductance of this device is 1.89 μS, after Pt metal deposition there is a negative shift in the zero bias conductance value and it becomes 1.08 μS. This negative shift in zero bias conductance indicates Fermi level re-alignment and tunneling of carriers after Pt deposition at the top most layer. To the best of our knowledge, this is the first report of such negative conductance after Pt metal deposition on graphene and this may have important implications such as in the fabrication of tunneling devices using graphene. However, this negative conductance could not be verified with the other devices. Moreover, it should be noted that the high bias conductance after every step of Pt deposition is always positive.

dx.doi.org/10.1021/am400489y | ACS Appl. Mater. Interfaces 2013, 5, 3424–3430

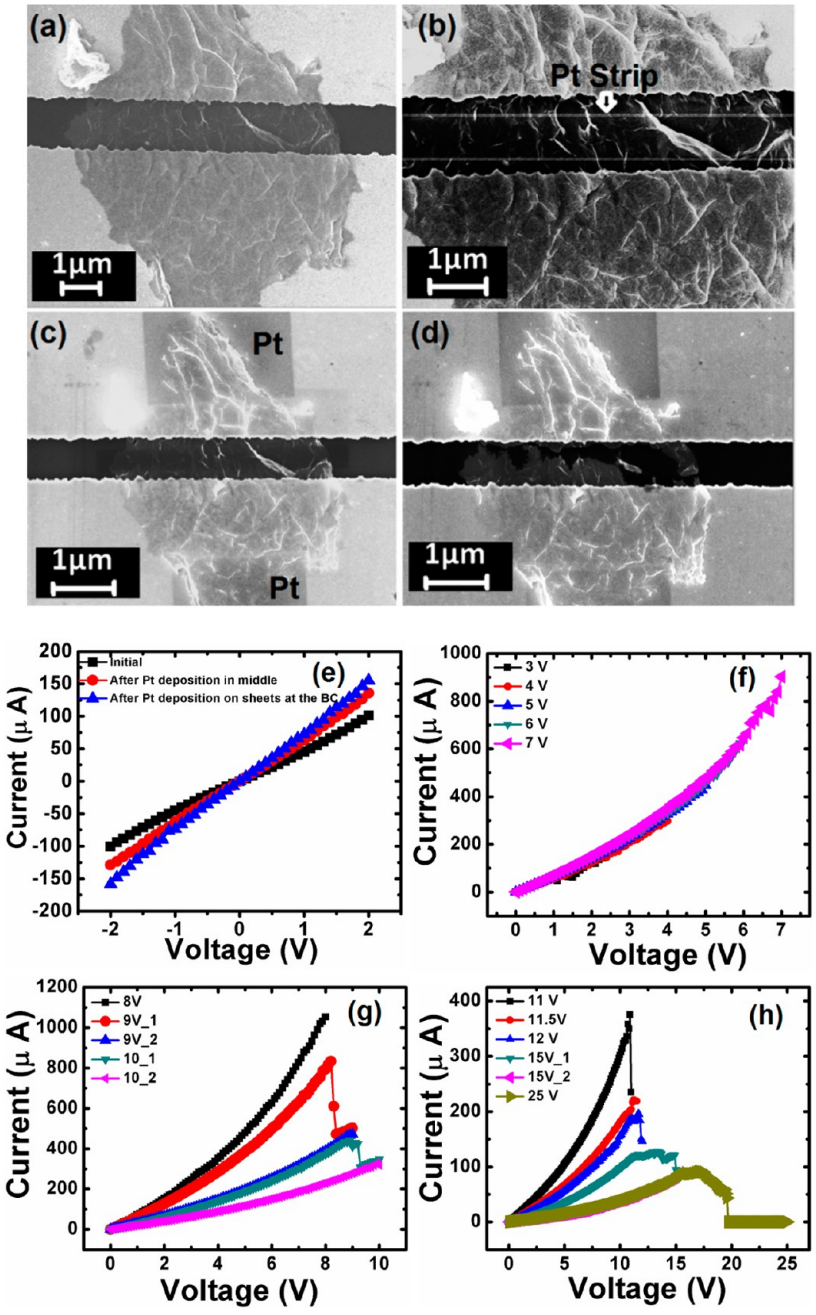

Figure 5. (a) SEM image of graphene sheets suspended between two gold electrodes, (b) same sheets after Pt metal deposition at the middle, (c) after Pt metal deposited at the two sides of sheets on bottom electrodes, (d) SEM image after the breakdown of the graphene sheet device, (e) *I*−*V* curves of the graphene sheet device corresponding to the different situations of Pt metal deposition, (f) *I*−*V* curves for higher voltage range, (g, h) *I*−*V* curves of the graphene sheet device till breakdown.

For the present device, the current increases at higher biases (shown in Figure 4g) and at 6 V, the current reaches up to 490 μA. An abrupt decrease in current of the device has been observed at 6.4 V, indicating the onset of the failure of graphene−Pt composite sheets; however, the current has not entirely vanished, as shown in the inset of Figure 4g. Breakdown of the sheets is confirmed by SEM imaging (Figure 4d). Interestingly, the Pt strip has been found to be converted to the discrete Pt nanoparticles during joule heating induced breakdown of the sheets. The breakdown of this graphene sheet device is somewhat different from the previous case (Figure 3) as all the graphene sheets are not burnt completely and are thus causing a non-vanishing current as indicated in *I*−*V* measurements. This graphene flake has much less area on the bottom contacts, and hence the electrodes are not efficient heat removers; however, the effective contact areas are almost similar at the two Au electrodes. Hence the maximum temperature rise is expected at the middle of the two contacts. We expect a temperature rise of around 500−700 °C in the middle to convert the EBID deposited continuous metal strip to Pt nanoparticles. These particles embedded in the broken graphene debris are magnified in the inset of Figure 4d.

In the next experiment (Figure 5), to completely exclude the contribution of contact improvement in the electrical conduction, now first the Pt strip has been deposited at middle excluding the contacts (Figure 2; Gr3 in schematic II). The

current at 2 V for this case has been found to be 129 μA as compared to the initial (without any metal deposition) current value of 100 μA (Figure 5e). The possible explanation for this improvement is the Pt intercalation and hence the doping of charge carriers in the graphene sheets leading to increased interlayer interaction. After Pt metal deposition at the two edges of the same sheet at the contacts (Figure 2; see Gr3 in III), the current further increases to 158 μA at 2 V. The corresponding zero bias conductances are 50.71, 68.22, and 79.39 μS, respectively, for the above mentioned situations. The maximum current for this device is about 1 mA at 8 V. After 8 V sweep, a stepped breakdown of the sheets has been observed as shown in figure 5g, h. It is important to mention here that for this device the breakdown starts at higher voltage as compared to the graphene sheet devices shown in figure 3 (breakdown voltage ~6.2 V) and figure 4 (breakdown voltage ~6.4 V). For this graphene sheet, formation of Pt nanoparticles, is not observed, unlike the case in Figure 4, in spite of the higher bias. This is a direct evidence of temperature rise in the previous case (Figure 4) occurring due to joule heating because of high contact resistance caused by less contact area. One can compare the effective contact area of graphene on the two electrodes with the relative spacing between them for the graphene sheets shown in Figures 4 and 5. In Figure 4, a much smaller area of the sheets is at the contacts, whereas in the present case (Figure 5), the graphene−metal contact area is large. Because of this large contact region of graphene with bottom electrodes, a stepped breakdown is observed for this device. In this case, the contacts behave as good heat sinks and the heat is efficiently removed which prevents the abrupt rise in the temperature and sheet by sheet breakdown is observed. The type of breakdown information is important as the layer by layer peeling of graphene at high temperatures caused by large biases has been reported to produce monolayer graphene at local sites.[21] However, the high temperature may also induce the simultaneous burning of more than one or two sheets also.

On the basis of electrical data obtained for different graphene sheet devices, we can conclude that the contact improvement is not the sole reason for the improved electrical conduction after top metal deposition as the enhancement in the conduction is observed irrespective of the fact that deposition site include the bottom contact or not. For example, in both the experiments (Figure 4 and 5), a significant contribution in improved electrical conduction comes even if the bottom contacts are excluded from the deposition. In case of multilayer graphene, the bottom-most sheet is in the direct contact with the bottom metal electrodes via weak Van der Waal bonding between Au and carbon atoms as well as amongst the sheets themselves. At room temperature and low bias voltages the electrons travel in-plane and the conduction through the other sheets is possible only by out-of-plane tunneling of the charge carriers which may occur at high bias voltages. In the present study, the improved electrical performance of the graphene sheets even at the zero bias, after the deposition of Pt metal at the middle (and thus excluding the contribution of contact improvement) can be explained in terms of diffusion of metal from top most layer to other layers and thereby enhancing the vertical tunneling of the charge carriers assisted by diffused metal particles. Evidence of diffusion of metal clusters in graphitic network of multiwalled Carbon nanotubes, causing increased conductance has been already published by our group.[22] Diffusion of metal atoms in the hexagonal network of MWNTs has also been discussed by Banhart.[23] However it should be noted that in CNT the similar outermost shell at which the metal is deposited, comes in direct contact of bottom electrode while in case of graphene multilayers, metal is being deposited at the top most layer while the bottom most layer is in direct contact of bottom metal electrodes. Hence the diffusion of metal becomes more clear in case of graphene sheets. Further, the graphene flakes produced by thermal exfoliation and reduction of graphite oxide are defective in nature and these defects such as vacancies present in the graphene lattice also assist the Pt diffusion among graphene layers. From high-resolution transmission electron microscope (HRTEM) image of platinum deposited graphene sheets, the intercalation of platinum nanoclusters amongst the graphitic sheets becomes quite clear (Figure 6).

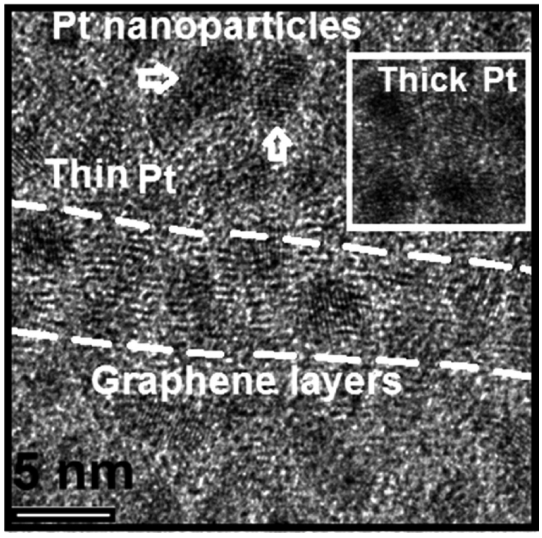

Figure 6. Transmission electron microscope (TEM) image of Pt deposited on multilayer graphene sheets by electron beam induced deposition. The graphene multilayers are demarked by two white dashed lines. The platinum nanoclusters are seen to be intercalated in graphene layers. Note that for the HRTEM investigation, deliberately very thin Pt was deposited to show the Pt nanoclusters as well as graphitic layers. For thick metal deposition only the dark contrast in image is visible not the graphitic layers as shown in the inset of the figure.

For TEM analysis, the metal on graphene sheets has been deposited using the same EBID technique however the thickness of the deposited metal has been deliberately kept low so as to meet the sample requirement for TEM analysis.[21] Otherwise the graphene sheets would not be visible and the area covered by dark continuous nanoclusters of the Pt film will only be visible (inset in Figure 6). Because of the low thickness of the deposited Pt metal, the Pt is appearing in the nanoclusters form in these TEM images.

To summarize, we have experimentally demonstrated that the Pt metal−graphene interaction causes a significant improvement in the electrical properties of multilayer graphene sheets. This improvement includes the contact improvement as well as increased interlayer interaction and is explained in terms of the doping of graphene sheets caused by the charge transfer between the deposited metal and the graphene and thus increasing the available density of states for electrical conduction. This experimental approach directly demonstrate that the contact improvement is not the sole reason for the improved electrical conduction as the improvement has been observed even when the metal is deposited on the part of the

graphene sheets not touching the bottom metal contacts and hence the contribution caused by increased interlayer interaction in overall improvement is segregated. The intercalated Pt nanoclusters within the sheets facilitate the vertical tunneling of the charge carriers in the graphitic planes. The two types of breakdown behaviors viz. sharp and stepped breakdowns are observed for these graphene sheets. These breakdown behaviors are explained in terms of the effective graphene-metal contact area. If the sheets make good contact with electrodes then the critical breakdown current densities in milliampere current range (typically 1 mA/μm) with a stepped breakdown is observed, otherwise a sharp breakdown is observed. The approaches presented in this study are important for characterization of devices incorporating graphene and metal contacts and lead to improved fundamental understanding of a variety of graphene-based device applications.

4. EXPERIMENTAL SECTION

Graphene Flake Preparation. The graphene flakes were obtained by the oxidation of micrometer size graphitic pieces, then reducing the obtained graphite powder by thermal reduction. More details can be found in ref 16. The flakes were ultrasonicated in isopropyl alcohol for several hours for their separation and dispersed on the gold electrodes for electrical characterization. The HRTEM images and electron diffraction patterns were obtained using JEOL JEM 2100 F operated at 200 KeV. The Raman spectra of the samples were obtained using instrument Horiba Jobin Yvon, HR800 with the spot size of laser beam being100 μm and excitation wavelength 514 nm.

Contact Formation for *I*–*V* Measurements. A metal (Cr/Au) layer of 200 nm on Si/SiO2 (150 nm) and PMMA 950 kA 2% have been used for patterning the electrodes. Bottom contact pads have been directly written using electron beam lithography in Raith 150-TWO direct write setup. Spacing in contact pads has been achieved by wet etching of Au and Cr. The graphene flakes have been transferred on the so achieved patterns in order to have them suspended between the two random pads. The platinum metal has been deposited on the sheets using gas injection system available in the same Raith150-TWO direct write setup. Electron beam induced deposition (3 KeV) of platinum is achieved using organo metallic precursor trimethyl-methylcyclopentadienyl-platinum IV [$(CH_3)_3(CH_3C_5H_4)$ Pt].

Electrical Characterization. Current–voltage characteristics of the graphene sheet devices were obtained using Keithley 4200 source meter using two probe configuration. The voltage sweep program was used to obtain current through the sheets in the predefined voltage range.

AUTHOR INFORMATION

Corresponding Author

*E-mail: nehaphysics@gmail.com.

Notes

The authors declare no competing financial interest.

ACKNOWLEDGMENTS

The authors acknowledge the Centre for Excellence in Nanoelectronics (CEN), IITB, for SEM imaging, lithography, and electrical measurements and Sophisticated Analytical Instrument Facility (SAIF) for high-resolution transmission microscopic (HRTEM) imaging.

REFERENCES

(1) Novoselov, K. S.; Geim, A. K.; Morozov, S. V.; Jiang, D.; Zhang, Y.; Dubonos, S. V.; Grigorieva, I. V.; Firsov, A. A. *Science* **2004**, *306*, 666.

(2) Zhang, Y.; Tan, Y. W.; Stormer, H. L.; Kim, P. *Nature* **2005**, *438*, 201.

(3) Lee, S.; Wijesinghe, N.; Diaz-Pinto, C.; Peng, H. *Phys. Rev. B.* **2010**, *82*, 045411.

(4) Nagashio, K.; Moriyama, T.; Ifuku, R.; Yamashita, T.; Nishimura, T.; Toriumi, A. *IEDM* **2011**, *978*, 27.

(5) Giovannetti, G.; Khomyakov, P. A.; Brocks, G.; Karpan, V. M.; Van den Brink, J.; Kelly, P. J. *Phys. Rev. Lett.* **2008**, *101*, 026803.

(6) Gong, C.; Lee, G.; Shan, B.; Vogel, E. M.; Wallace, R. M.; Cho, K. *J. Appl. Phys.* **2010**, *108*, 123711.

(7) Pi, K.; McCreary, K. M.; Bao, W.; Han, W.; Chiang, Y. F.; Li, Y.; Tsai, S. W.; Lau, C. N.; Kawakami, R. K. *Phys. Rev. B.* **2009**, *80*, 075406.

(8) Santos, J. E.; Peres, N. M. R.; Lopes dos Santos, J.M.B.; Castro Neto, A. H. *Phys. Rev. B.* **2011**, *84*, 085430.

(9) Iqbal, M W.; Singh, A. K.; Iqbal, M Z.; Eom, J. *J. Phys. Condens. Matter.* **2012**, *24*, 335301.

(10) Murali, R.; Brenner, K.; Yang, Y.; Beck, T.; Meindl, J. D. *IEEE Elec. Dev. Lett.* **2009**, *30*, 611.

(11) Lee, K. J.; Chandrakasan, A. P.; Kong, J. *IEEE Electron. Dev. Lett.* **2010**, *32*, 557.

(12) Venugopal, A.; Colombo, L.; Vogel, E. M. *Appl. Phys. Lett.* **2010**, *96*, 013512.

(13) A. Barreiro, A.; Lazzeri, M.; Moser, J.; Mauri, F.; Bachtold, A. *Phys. Rev. Lett.* **2009**, *103*, 076601.

(14) Lin, Y. M.; Dimitrakopoulos, C.; Farmer, D.B.; Han, S. J.; Wu, Y.; Zhu, W.; Kurt Gaskill, D.; Tedesco, J. L.; Myers-Ward, R. L.; Eddy, C. R., Jr; Grill, A.; Avouris, P. *Appl. Phys. Lett.* **2010**, *97*, 112107.

(15) Cao, H.; Yu, Q.; Jauregui, L. A.; Tian, J.; Wu, W.; Liu, Z.; Jalilian, R.; Benjamin, D. K.; Jiang, Z.; Bao, J.; Pei, S. S.; Chen, Y.P. *Appl. Phys. Lett.* **2010**, *96*, 122106.

(16) Rafiee, M. A.; Rafiee, J.; Srivastava, I.; Wang, Z.; Song, H.; Yu, Z. Z.; Koratkar, N. *Small* **2010**, *6*, 179.

(17) Meyer, J. C.; Geim, A. K.; Katsnelson, M. I.; Novoselov, K. S.; Booth, T. J.; Roth, S. *Nature* **2007**, *446*, 60.

(18) Ferrari, A.C.; Robertson, J. *Phys. Rev. B.* **2000**, *61*, 14095.

(19) Kuroda, M. A.; Leburton, J. P. *Appl. Phys. Lett.* **2006**, *89*, 103102.

(20) Santini, C. A.; Vereecken, P. M.; Volodin, A.; Groeseneken, G.; Gendt S., De.; Haesendonck, V. *IOP Nanotechnol.* **2011**, *22*, 395202.

(21) Barreiro, A.; Borrnert, F.; Rummeli, M. H.; Buchner, B.; Vandersypen, L. M. K. *Nano Lett.* **2012**, *12*, 1873.

(22) Kulshrestha, N.; Misra, A.; Bajpai, R.; Roy, S.; Misra, D. S. *IEEE Trans. Nanotechnol.* **2012**, *11*, 4830.

(23) Banhart, F. *Nanoscale* **2009**, *1*, 201.